



Surface enhanced Raman scattering investigation of two novel Piperazine carbodithioic acids adsorbed on Ag and ZnO nanoparticles

Journal:	<i>RSC Advances</i>
Manuscript ID:	RA-ART-10-2014-012928.R1
Article Type:	Paper
Date Submitted by the Author:	01-Dec-2014
Complete List of Authors:	<p>Singh, Ranjan; Banaras Hindu University, Physics Prakash, Om; Banaras Hindu University, Varanasi- 221105, Department of Physics Gautam, Priyanka; Banaras Hindu University, Varanasi- 221105, Department of Physics Kumar, Shiv; Banaras Hindu University, Varanasi- 221105, Department of Physics Singh, Pushkar; Leibniz Institute of Photonic Technology, Albert-Einstein-Straße 9, 07745 Jena, Germany., Leibniz Institute of Photonic Technology, Albert-Einstein-Straße 9, 07745 Jena, Germany. Dani, R.; Banaras Hindu University, Chemistry Bharty, Manoj; Banaras Hindu University, Chemistry Singh, Nand; Banaras Hindu University, Chemistry Ghosh, Anup K.; Banaras Hindu University, Department of Physics Deckert, V; Leibniz Institute of Photonic Technology, Albert-Einstein-Straße 9, 07745 Jena, Germany, Institute of Physical Chemistry and Abbe Center of Photonics, Friedrich-Schiller University, Helmholtzweg 4, 07743 Jena, Germany, Leibniz Institute of Photonic Technology, Albert-Einstein-Straße 9, 07745 Jena, Germany, Institute of Physical Chemistry and Abbe Center of Photonics, Friedrich-Schiller University, Helmholtzweg 4, 07743 Jena, Germany</p>

Cite this: DOI: 10.1039/c0xx00000x

www.rsc.org/xxxxxx

ARTICLE TYPE

Surface enhanced Raman scattering investigation of two novel Piperazine carbodithioic acids adsorbed on Ag and ZnO nanoparticles

Om Prakash^a, Priyanka Gautam^a, Shiv Kumar^a, Pushkar Singh^c, R. K. Dani^b, M. K. Bharty^b, N. K. Singh^b, A. K. Ghosh^a, V. Deckert^{c,d}, Ranjan K. Singh^{a*}

Received (in XXX, XXX) Xth XXXXXXXXX 20XX, Accepted Xth XXXXXXXXX 20XX
DOI: 10.1039/b000000x

In this work Piperazine -1-carbodithioic acid (PZCDT) and Piperazine -1, 4-carbodithioic acid (PZbCDT) were synthesized. These analytes *viz.* PZCDT & PZbCDT have chaired conformer which is expected to give specific surface-enhanced Raman scattering (SERS) effects on individual bands. The SERS, UV-Visible, TEM and DFT methods have proved that the dithiocarbamate moiety is a potential and competent functional group for silver and ZnO nanoparticles (AgNPs and ZnONPs). The enhancement mechanism and enhancement factors in both SERS@AgNPs and SERS@ZnONPs have also been discussed. Two new strong bands are appeared at 1630, 1286 cm⁻¹ with very large intensity in SERS@AgNPs which signify the conversion of C-N bond of dithiocarbamate moiety into C=N bond. SERS signatures are observed quite different in two; SERS@AgNPs and SERS@ZnONPs.

Introduction:

Surface enhanced Raman scattering (SERS) is a surface sensitive technique that results in considerable enhancement of certain Raman bands when the scattering molecules are adsorbed on rough metallic surfaces. The intensity enhancement in SERS is high enough in certain favourable cases to bring Raman technique at par with fluorescence technique to detect materials in trace amount/ single molecule.¹⁻⁴ SERS is thus a sensitive technique for detecting molecular species and it is useful to investigate the characteristic properties of molecular species in biological, chemical, material, medicinal, agricultural sciences.^{5,6} SERS is an effective technique in studying surface-interfacial properties and has ability to detect multiple analytes using overlayer technique.⁷ SERS effect is based mainly on two mechanisms, one a long-range electromagnetic (EM) effect and the other a short range charge transfer (CT) effect also called as chemical (CHEM) enhancement effect.⁷⁻⁹ The EM enhancement is based on the increase in the local electric field around the metal-molecule adsorbed system. The charge transfer (CT) mechanism is based on the photo-induced transfer of an electron from the Fermi level of the metal to an unoccupied molecular orbital of the adsorbate or vice versa, depending on the energy of the photon and electric potential of the interface. The total enhancement in SERS is product of two mechanism (EM and CT).¹⁰⁻¹¹ The SERS enhancement depends on type of SERS substrate, degree of roughness of surface, size and shape of substrate and most importantly the employed laser excitation energy. The detail theory of the enhancement mechanism in SERS has been explained in many literatures.⁷⁻⁹

The present work has been studied in following sequences – synthesis of two novel analytes; Piperazine -1-carbodithioic acid (PZCDT) and Piperazine -1, 4-carbodithioic acid (PZbCDT)

specially, then the adsorption/ binding sites of PZCDT and PZbCDT have been analyzed on two different kind of substrate; silver nanoparticles (AgNPs) and ZnO nanoparticles (ZnONPs) and thereafter SERS study has been performed. The DFT calculation, average orientation of vibration vectors, vibrational assignments and potential energy distribution are done with the help of Gaussian 03, GaussView and GAR2PED software.

3D (XYZ) demonstration of PZCDT and PZbCDT ions:

The orientation of adsorbate on substrate is an important factor in SERS to decide the intensity enhancement of vibrational modes and to apply the SERS surface selection rule.^{7,10,11,14-16} In adsorption phenomena, both the functional group as well as the structure of adsorbate is significant. The 3-dimensional geometries of PZCDT and PZbCDT ions are demonstrated in Fig. 1. Both PZCDT and PZbCDT ions consist of a six-membered ring (PZ ring) containing two nitrogen atoms at opposite positions in the ring giving them privileged structures that contain non-planar part different from other widely studied analytes *viz.* pyridine, adenine, benzenethiol derivatives etc.¹⁷⁻²² The – N site of PZ ring (after removal of H atom) is associated to – dithiocarbamate moiety.

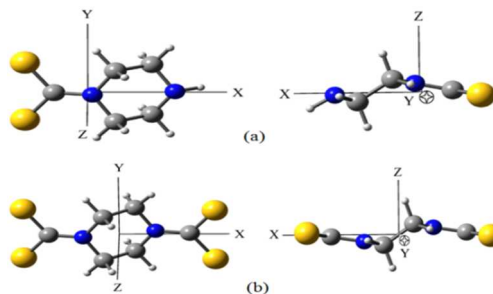


Fig.[1]: 3D (XYZ) demonstrations of (a) PZCDT and (b) PZbCDT ions.

Results and discussions:

In order to understand the experimental results, it is noteworthy to reveal first of all the interaction/ coordination of PZCDT & PZbCDT with AgNPs and ZnONPs and their respective orientation as it is significant factor for SERS.^{23, 24} In this order, DFT computations have been performed (See – DFT analysis). The optimized geometry of PZCDT and PZbCDT with silver cluster is shown in Fig 2. The vibrational modes are assigned with the help of Gaussian 03, Gauss View 4.1 and GAR2PED software.^{25, 26} as given in Table 1 and also with help of some reported results.²⁷⁻²⁹

Spectral analysis of SERS@AgNPs of PZCDT and PZbCDT:

Before analysing the Raman spectra and intensity enhancement in SERS, it should be worth commenting that charge transfer phenomena usually occur through the chemical adsorption. It is well known that when the complexes (substrate + adsorbate) are irradiated with laser source then few new bands appear if adsorbates have enough energy and on the other hand if adsorbates have not enough energy then this results in disappearance of few bands.^{10, 11} However, it should be mentioned that SERS results also significantly depend on the orientation of vectors of corresponding vibrational modes.

The normal Raman spectra of PZCDT and PZbCDT and their SERS spectra adsorbed on AgNPs (SERS@AgNPs) are measured in region 200-3500 cm^{-1} . To identify the subtle changes in SERS spectra, the experimental spectra are truncated in two regions; 1150-1750 cm^{-1} and 200-1160 cm^{-1} as shown in Fig. 3(a) and (b). The $\nu(\text{C-H})$ (symmetric/ asymmetric) bands of PZ ring disappeared in SERS spectra of both PZCDT and PZbCDT because the vector of $\nu(\text{C-H})$ vibrations is nearly parallel to Ag surface. In region 1150-1750 cm^{-1} , we observed drastic changes in SERS spectra compared to the normal Raman spectra. Two very strong new bands at 1630 and 1286 cm^{-1} are observed in both PZCDT and PZbCDT. Actually the appearance of the bands at 1630 and 1286 cm^{-1} is due the formation of C=N bond from C-N bond via adsorption catalysis. In adsorption catalysis, the charge transfer occurs from silver atom (positive charge) to deprotonated S \cdots C \cdots S region (negative charge), this results into conversion of C-N bond to C=N bond. The band at 1630 cm^{-1} is mainly due to C=N stretching. The vibration vector of $\nu(\text{C=N})$ is oriented exactly normal to Ag surface. Similarly the new band at 1286 cm^{-1} is again mainly due to C=N bond and attributed to the $\beta(\text{C-C=N})$ with additional contribution of $\rho(\text{CH}_2)_{\text{upper}}$ of PZ ring. Here $\rho(\text{CH}_2)$ vector is also perpendicular to surface of Ag film. The appearance of these bands confirms the adsorption process. The band at 1409 cm^{-1} ($w(\text{CH}_2)_{\text{lower}} + \nu(\text{C-C})$) whose vibration vector is tilted, is enhanced and broadened in SERS centred at 1412 cm^{-1} (PZCDT) and 1406 cm^{-1} (PZbCDT).

The band at 1354 cm^{-1} attributed to wagging (W) of CH_2 is observed in normal Raman spectra of both PZCDT and PZbCDT but in SERS spectra, it splits into two components centred at 1362 ($W(\text{CH}_2) + \nu(\text{C=N})$) and 1348 cm^{-1} ($\gamma(\text{CH}_2) + \beta(\text{C-N=C})$) in PZCDT and, at 1365 ($W(\text{CH}_2) + \nu(\text{C=N})$) and 1348 cm^{-1} ($\gamma(\text{CH}_2) + \beta(\text{C-N=C})$) in PZbCDT.

Table 1: Experimentally observed Raman and SERS@Ag bands (in cm^{-1}) and their tentative vibrational assignments of PZCDT and PZbCDT (1750 - 200 cm^{-1}):

S.N	Raman	SERS@Ag		Vibrational assignments
		PZCDT	PZbCDT	
1	---	1630	1630	$\nu(\text{C=N})$
2	1461	1460	---	$\beta_{\text{scis}}(\text{CH}_2)$
3	1409	1412	1406	$W(\text{CH}_2)_{\text{lower}} + \nu(\text{C-C})$
4	---	1362	1365	$W(\text{CH}_2) + \nu(\text{C=N})$
5	1354	---	---	$W(\text{CH}_2)$
6	---	1348	1348	$\gamma(\text{CH}_2) + \beta(\text{C-N=C})$
7	---	1286	1286	$\beta(\text{C-C=N}) + \rho(\text{CH}_2)_{\text{upper/PZ ring}}$
8	1218	1218	1218	$\nu(\text{C-N}) + \gamma(\text{CH}_2) + \beta_{\text{LIN}}(\text{C-N=C}) + W(\text{CH}_2)_{\text{upper}}$
9	1118	1126	1126	$\nu(\text{C-N})_{\text{ring}} + \nu(\text{C-C})$
10	1086	---	---	$\delta_{\text{TRI}}(\text{PZ}) + \beta_{\text{OUT}}(\text{NH}) + \rho(\text{CH}_2)$
11	---	888	888	$\beta(\text{C-C=N}) + \beta(\text{S-C-S}) + \nu(\text{C-N}) + \delta_{\text{TRI}}(\text{RING})$
12	---	727	727	$\beta(\text{S-C-S}) + \Phi(\text{ring})_{\text{PZ}}$
13	568	562, 580	562, 580	$\text{LIN}(\text{N-C-S}) + \delta_{\text{TRI}}(\text{RING}) + \delta_{\text{ASYM}}(\text{Ring}) + \nu(\text{CS}) + \beta_{\text{OUT}}(\text{N-H}) + \tau_{\text{ASYM}}(\text{Ring}) + \nu(\text{C-N})_{\text{ring}}$
14	531	512	512	$\delta_{\text{TRI}}(\text{Ring}) + \delta_{\text{ASYM}}(\text{Ring}) + \beta_{\text{OUT}}(\text{N-H}) + \text{LIN}(\text{C-N-C})$
15	401	---	---	$\tau(\text{C-N})_{\text{ring}} + \tau(\text{C-C})_{\text{ring}} + \text{LIN}(\text{N-C-S}) + \tau(\text{CH}_2) + \tau(\text{NH})$
16	---	394	394	$\delta_{\text{ASYM}}(\text{Ring}) + \text{LIN}(\text{NCS}) + \nu(\text{Ag-S}) + \beta(\text{C-S-Ag})$
17	380	---	---	$\delta_{\text{ASYM}}(\text{Ring}) + \text{LIN}(\text{N-C-S})$

ν = stretching, β = bending, γ = twisting, W = wagging, ρ = rocking, δ = deformation, τ = torsion, Φ = ring breathing, LIN = linear bending, TRI = trigonal bending, OUT = out of plane, SYM = symmetric, ASYM=asymmetric

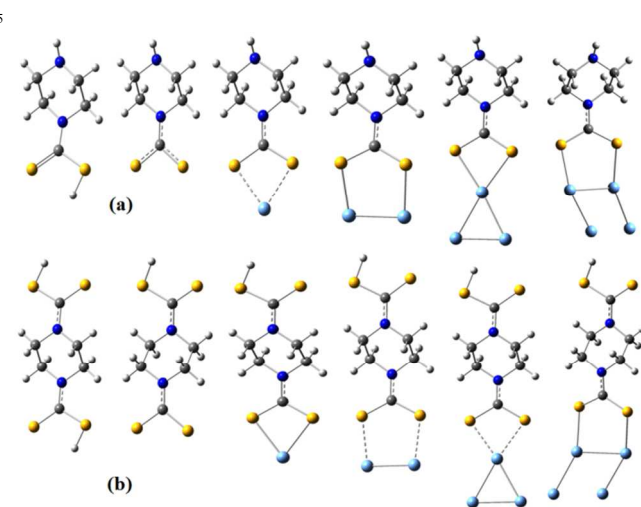


Fig. 2: (a) Optimized structures of PZCDT, deprotonated PZCDT, and PZCDT+Ag_{n=1, 2, 3, 4}, (b) Optimized structures of PZbCDT, deprotonated PZbCDT, and PZbCDT+Ag_{n=1, 2, 3, 4},

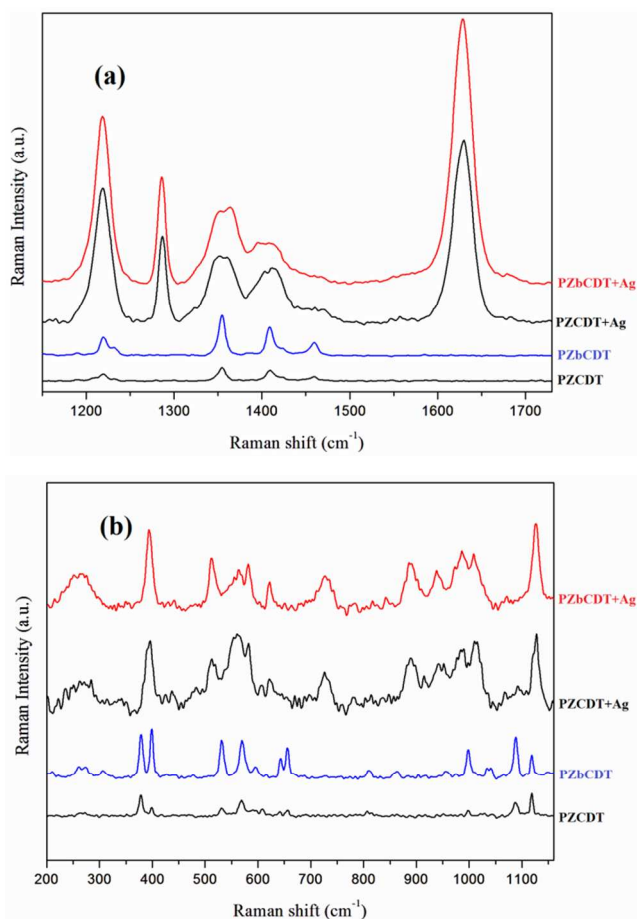


Fig.[3]: Baseline corrected experimental normal Raman and SERS@AgNPs spectra of PZCDT and PZbCDT in region (a) 1150 – 1700 cm^{-1} and (b) 200 – 1150 cm^{-1} .

It is further interesting to note that the normal Raman band at 1220 cm^{-1} is enormously enhanced in the SERS spectra as shown in Fig. 3(a). The resultant vibration vector of mode $\nu(\text{C-N}) + \gamma(\text{CH}_2) + \beta_{\text{LIN}}(\text{C-N}=\text{C}) + \text{W}(\text{CH}_2)_{\text{upper}}$ is perpendicular to Ag surface therefore according to SERS selection rule the enhancement takes place. Although it is also well known that in SERS via chemisorptions the enhancement of SERS is mainly due to $\pi \cdots \pi^*$ transition (HOMO-LUMO).^{10,11,14,15} Further due to the charge transfer from AgNPs to dithiocarbamate moiety and PZ ring, the Raman bands at 1118 and 1086 cm^{-1} coupled in SERS spectra at 1126 cm^{-1} with increased intensity. The vibrational assignments of bands at 1118, 1086 and 1126 cm^{-1} are given in Table 1. Many bands in the region 200-1050 cm^{-1} are noted with different enhancement behaviour in two analytes PZCDT and PZbCDT unlike other regions. It is interesting to look into the reason behind it. As matter of fact this region mainly contains C-S stretching and trigonal deformation of PZ ring. Now it should be noted that PZCDT consists of one dithiocarbamate moiety and PZbCDT consists of two dithiocarbamate moiety (Fig 2). Due to this different charge cloud is associated with PZ ring of PZCDT and PZbCDT before as well as after the adsorption on AgNPs. Therefore we observed different Raman and SERS signatures in this region as shown in Fig 3b. In region 900 – 1000 cm^{-1} , some bands are enhanced. Two new bands appeared at 888 and 727 cm^{-1} in SERS and

assigned vibrational modes as given in Table 1. The vibration vectors of the bands at 888 and 727 cm^{-1} are perpendicular to silver surface as analyzed by GaussView. The appearing of these two bands is due to charge transfer from the silver particles to PZ ring via – dithiocarbamate moiety. The normal Raman band at 568 cm^{-1} is splitted in two components at 580 and 562 cm^{-1} with enhanced intensity in both PZCDT and PZbCDT. Similarly the intensity of normal band at 531 cm^{-1} is increased as shown in Fig. 3b. Both Ag and S atoms have promising nature to form covalent (coordinate) bond Ag-S. There are two bands in linear Raman spectra at 380 and 401 cm^{-1} containing $\delta\text{ASYM}(\text{Ring})+\text{LIN}(\text{NCS})$ and in SERS these two bands merge to 393 cm^{-1} band having contribution from $\delta\text{ASYM}(\text{Ring})+\text{LIN}(\text{NCS})+ \nu(\text{Ag-S})+ \beta(\text{C-S-Ag})$. This provides clear evidence of chemical bond formation between Ag and S atoms. In Fig. 3b, we also observed that the normal Raman bands in region 200 – 300 cm^{-1} are enhanced in SERS spectra. The SERS of two analytes reveals that dithiocarbamate moiety is adsorbing unit on Ag in both.

Spectral analysis of SERS@ZnONPs of PZCDT and PZbCDT:

The normal Raman and SERS@ZnONPs spectra of PZCDT and PZbCDT are measured in spectral region 200-3500 cm^{-1} . To analyse the changes precisely, the entire spectra have been truncated in three regions; 2650-3200 cm^{-1} , 1150-1750 cm^{-1} and 200-1160 cm^{-1} as shown in Fig. 4(a), (b) and (c).

The SERS spectra exhibited many signatures that indicate the adsorption of PZCDT and PZbCDT on ZnONPs. The detail vibrational assignments of normal Raman and SERS bands are given in Table 2. As expected the $\nu(\text{C-H})$ (symmetric/asymmetric) bands of PZ ring showed blue/ red shift and broadening on adsorption as shown in Fig. 4(a). However, the features are different for the two analytes because of difference in coordination with ZnO as shown in Fig ES4. The normal Raman bands at 1461 cm^{-1} are enhanced and shifted to 1461 and 1462 cm^{-1} in PZCDT and PZbCDT respectively. Similarly In PZbCDT, a strong band at 1409 cm^{-1} (having a shoulder band at 1423 cm^{-1}) is enhanced with broadening in SERS at 1424 cm^{-1} which contain two shoulder bands on either side at 1435 and 1419 cm^{-1} (Fig. 4(b)). The normal Raman bands of PZCDT at 1354 cm^{-1} corresponding to $\text{W}(\text{CH}_2) + \beta(\text{C}=\text{N}-\text{C})$ is unshifted with intensity enhancement in SERS whereas the Raman band of PZbCDT at 1354 cm^{-1} is red shifted to 1349 cm^{-1} with nearly same integrated intensity which signify that ZnO is coordinated on both side of PZbCDT and results in reducing the induced dipole moment /Raman activity of this band (C=N-C). Further the normal Raman band at 1220 cm^{-1} in both PZCDT and PZbCDT is considerably enhanced as shown in Fig. 4(b). The SERS enhancement feature at 1220 cm^{-1} is quite different from that observed in SERS@AgNPs (Fig. 3(a)).

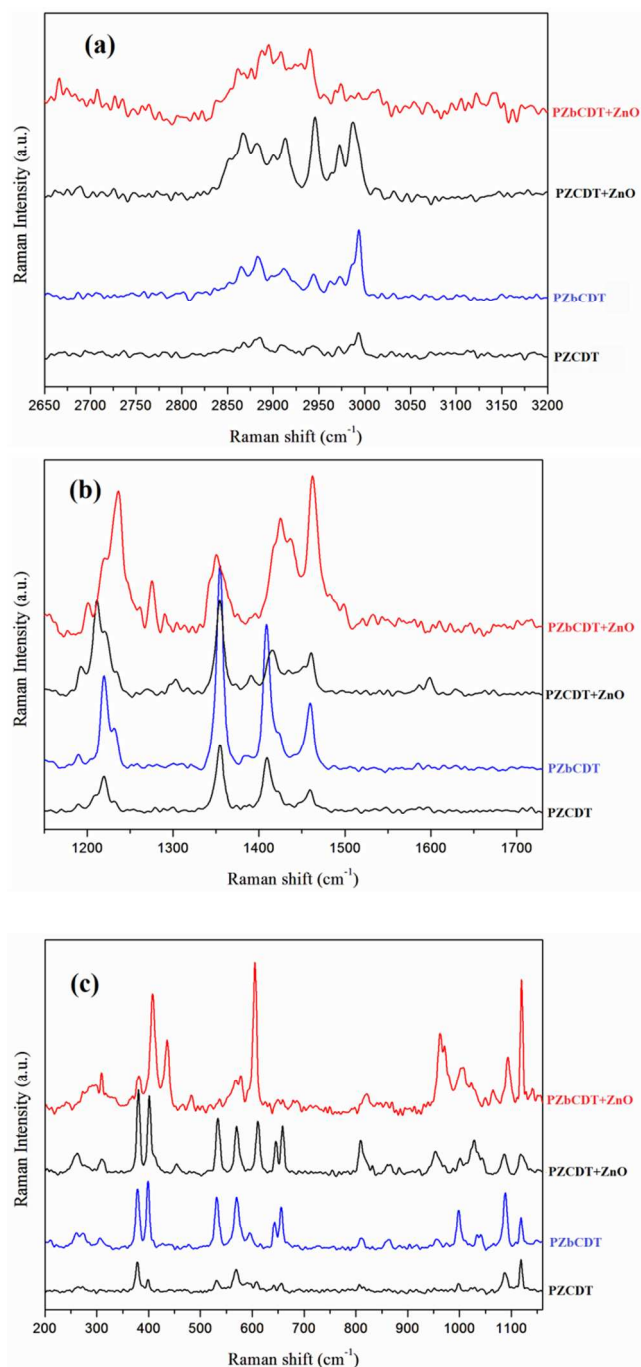


Fig. [4]: Baseline corrected experimental normal Raman and SERS@ZnONPs spectra of PZCDT and PZbCDT in region (a) 3200 – 2650 cm^{-1} , (b) 1730 – 1150 cm^{-1} and (c) 1160 – 200 cm^{-1} .

Moreover, the band at 1118 cm^{-1} is also enhanced in SERS spectra with unchanged frequency by a factor of 1.5 and 4.5 in PZCDT and PZbCDT respectively. Due to different molecular structures of PZCDT & PZbCDT and coordination properties with ZnO, the spectral feature of SERS is significantly different as shown in Fig. 4(c). Consequently, few new bands appeared at 1026, 956, 310 and 262 cm^{-1} with moderate intensity in SERS spectra of PZCDT and on other hand three prominent Raman bands at 656, 643 and 531 cm^{-1} are diminished in SERS spectra of PZbCDT (Fig. 4(c)). In PZCDT, few SERS enhanced bands are observed at 656, 643, 568, 531, 401 and 380 cm^{-1} with same

frequency as found in normal Raman spectra. The vibrational assignments of these bands are calculated as given in Table 2. It is noticeable that Raman bands at 609 and 401 cm^{-1} is shifted to 606 and 408 cm^{-1} and enhanced by factor of 17 and 3 respectively in SERS spectra of PZbCDT (Fig. 4(c)). A new band is observed at 435 cm^{-1} corresponding to vibrational modes $\nu(\text{Zn-S}) + \gamma(\text{PZ})$ in SERS spectra of PZbCDT and this confirms the formation of coordinate bond (Zn-S). The SERS signature of two normal Raman bands at 401 and 380 cm^{-1} in both PZCDT and PZbCDT is directly associated with Zn-S stretching (i.e. chelate ring Zn-S-C-S) which indicate the coordination of Zn-S bond. We also noticed that the spectral features of SERS@ZnONPs and SERS@AgNPs are quite different from each other. The causes behind it and a concise comparative study of enhancement mechanism and enhancement factor between two SERS@AgNPs and SERS@ZnONPs will be discussed in a forthcoming section.

Table 2: Experimentally observed Raman and SERS@ZnO bands (in cm^{-1}) and their tentative vibrational assignments of PZCDT and PZbCDT (1750 - 200 cm^{-1}):

S.N	Raman	SERS@ZnO		Vibrational assignments
		PZCDT	PZbCDT	
1	1461	1461	1462	$\beta_{\text{scis}}(\text{CH}_2)$
2	1409	1415	1424	$\text{W}(\text{CH}_2) + \nu(\text{C-C})$
3	1354	1354	1349	$\text{W}(\text{CH}_2)$
4	1220	1209	1236	$\gamma(\text{CH}_2)$
5	1118	1118	1118	$\nu(\text{C-N})_{\text{ring}} + \nu(\text{C-C})$
6	1086	1090	1090	$\delta_{\text{TRI}}(\text{RING}) + \beta_{\text{OUT}}(\text{NH}) + \rho(\text{CH}_2)$
7	809	819	820	$\beta_{\text{OUT}}(\text{N-H}) + \nu(\text{C-N})_{\text{ring}} + \rho(\text{CH}_2)$
8	656	656	---	$\beta_{\text{OUT}}(\text{C-N-C}) + \delta_{\text{TRI}}(\text{RING}) + \rho(\text{CH}_2) + \tau_{\text{ASYM}}(\text{RING})$
9	643	643	---	$\delta_{\text{TRI}}(\text{RING}) + \delta_{\text{ASYM}}(\text{RING}) + \nu(\text{C-S}) + \rho(\text{CH}_2)$
10	609	606	606	$\beta_{\text{OUT}}(\text{NCSS})$
11	568	568	568	$\text{LIN}(\text{N-C-S}) + \delta_{\text{TRI}}(\text{RING}) + \delta_{\text{ASYM}}(\text{RING}) + \nu(\text{C-S}) + \beta_{\text{OUT}}(\text{N-H}) + \tau_{\text{ASYM}}(\text{RING}) + \nu(\text{C-N})_{\text{ring}}$
12	531	---	---	$\delta_{\text{TRI}}(\text{RING}) + \delta_{\text{ASYM}}(\text{RING}) + \beta_{\text{OUT}}(\text{NH}) + \text{LIN}(\text{C-N-C})$
13	401	401	408	$\nu(\text{Zn-S}) + \tau(\text{C-N})_{\text{ring}} + \tau(\text{C-C})_{\text{ring}} + \text{LIN}(\text{N-C-S}) + \tau(\text{CH}_2) + \tau(\text{NH})$
14	380	380	382	$\nu(\text{Zn-S}) + \delta_{\text{ASYM}}(\text{RING}) + \text{LIN}(\text{N-C-S})$

ν = stretching, β = bending, γ = twisting, W = wagging, ρ = rocking, δ = deformation, τ = torsion, Φ = ring breathing, LIN = linear bending, TRI = trigonal bending, OUT = out of plane, SYM = symmetric, ASYM=asymmetric

Adsorption of dithiocarbamate moiety on ZnONPs -UV-Visible and TEM analysis:

The UV-Visible spectra of ZnONPs and complexes [ZnONPs + PZCDT/PZbCDT] are recorded to reveal the coordination properties possessed therein. The absorption band of ZnONPs is observed at 372 nm with band gap 3.3 eV, that is blue shifted when ZnO is coordinated to either PZCDT or PZbCDT. In PZCDT+ZnO complex the absorption band is observed at 265 nm, whereas two absorption bands at 283, 264 nm are observed in [PZbCDT+ZnO] as shown in Fig. 5.

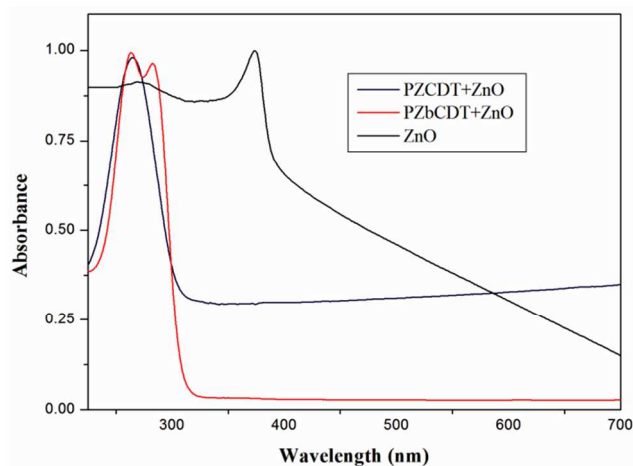


Fig.[5]: UV-Visible spectra of ZnONPs and complexes [ZnONPs + PZCDT/PZbCDT].

Two structured bands at 283, 264 nm give the clear evidence that ZnO is coordinated through dithiocarbamate on both side in [PZbCDT+ZnO] whereas on single side in [PZCDT+ZnO] via constructing a four membered chelate ring (Zn-S-C-S) which was also proved by DFT method (Fig.4). Further, the morphology and microstructure of pure ZnONPs, the complexes [PZCDT+ZnO] and [PZbCDT+ZnO] have been examined by transmission electron microscopy (TEM) to know the adsorption of PZCDT/PZbCDT on ZnONPs (see ES2).

The UV-Visible, TEM and SERS techniques confirmed that dithiocarbamate moiety could be used as the functional group for ZnONPs. Similarly, the results obtained through SERS@AgNPs reveal that dithiocarbamate moiety could also be used as the functional group for AgNPs. Many works have also been reported related to functional group of Ag/Au and ZnONPs.^{30,31} The resulting capped/ functionalised AgNPs owe the potential applications in biomedical research. It is also used frequently as catalytic agent in chemical and biological reactions.^{32,33} On the other hand, ZnONPs is better biocompatible than AgNPs and reliable on account of cost, reproducibility and toxicity therefore it would be more promising candidate to substitute AgNPs in complement as well as supplement aspect.

SERS@AgNPs Vs SERS@ZnONPs - Enhancement mechanism and enhancement factor:

In this section, we present a comparison of SERS characteristic from two different categories of substrates, metal and

semiconductor, concisely. The plasmon resonance frequency for AgNPs and ZnONPs lie in visible and infrared region respectively. The excitation source used for SERS is 514.15 nm line of Ar⁺ laser therefore EM mechanism is effective only in SERS@AgNPs but not effective in SERS@ZnONPs. The CHEM/CT enhancement mechanism is effective in both cases according to Otto's and Persson's models.^{39, 40}

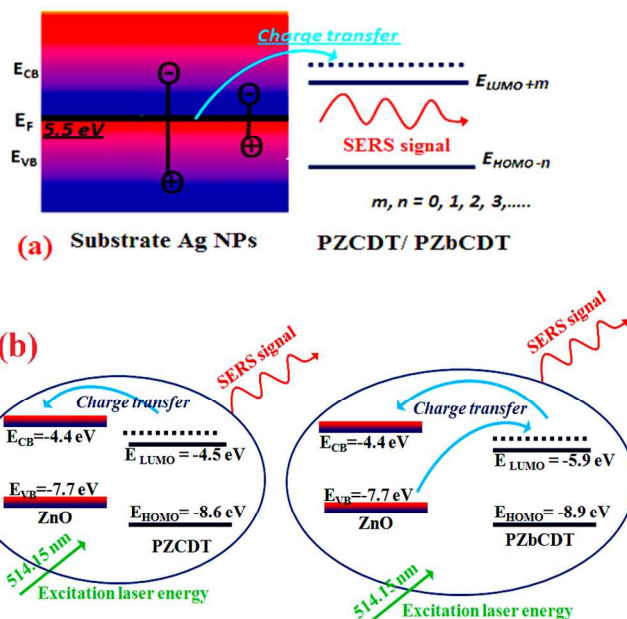


Fig.[6]: Schematic representation of suggested charge transfer mechanism in (a) SERS@AgNPs and (b) SERS@ZnONPs.

The CT enhancement mechanism in SERS process from two different kinds of substrates AgNPs and ZnONPs are illustrated schematically in Fig. 6(a) and (b). The energy levels of the HOMO and LUMO with respect to the Fermi level of AgNPs (5.5 eV) and ZnONPs (5.25 eV) are suitable (Fig.6) for charge transfer between the adsorbate and substrate causing increase in rate of change of polarizability during few vibrational modes of molecules. It should be noted that any of HOMOs – LUMOs (HOMO-n, where n = 0, 1, 2, 3... and LUMO+m, where m = 0, 1, 2, 3...) may cause the charge transfer. We also found that the energy gap of HOMO – LUMO (4.1 eV-PZCDT/ 3.0 eV-PZbCDT) is not equal to employed laser excitation energy (2.4 eV) i.e. resonance Raman enhancement does not take place.^{34, 35} The CT mechanism in SERS@ZnONPs is also investigated for both adsorbates. It is well known that conduction band (CB) and valence band (VB) of ZnONPs are at -4.4eV and -7.7eV respectively. It is found that the energy level of VB of ZnONPs is greater than HOMO value and CB is greater than LUMO value for both PZCDT and PZbCDT (Fig. 6(b)). According to Otto's and Persson's models, the charge transfer takes place from the LUMO level to CB of ZnO for PZCDT whenever for PZbCDT, charge transfer takes place via two path one; from the LUMO level to CB of ZnO and second; from the VB to LUMO level, as illustrated in Fig. 6(b). This CT mechanism changes the electronic structure of adsorbates and surface structure of ZnONPs thereby this affects the polarizability of adsorbates. Therefore Raman activity as consequence of SERS signal is amplified.

For quantitative comparison, the enhancement factor (EF) of SERS bands with respect to their corresponding normal Raman bands has been estimated. The accurate value of EF is calculated according to the equation $EF = (I_{SERS}/I_{NR}) \times (N_{NR}/N_{SERS})$, where N_{NR} and N_{SERS} are number of molecules taking part in normal Raman and SERS signal respectively and I_{SERS} and I_{NR} are integrated intensities.³⁶ An alternative way to estimate enhancement is analytical enhancement factor (AEF). The AEF is defined as $AEF = (I_{SERS}/I_{NR}) \times (C_{NR}/C_{SERS})$, where C_{NR} and C_{SERS} are molar concentration of solutions used for the normal Raman and SERS respectively.^{37,38} Since molar concentration of solutions are directly proportional to the number of molecules present in solutions therefore AEF is proportional to EF. There is a probability of error in instrumentation and in spectral measurement therefore the estimation of N_{NR} and N_{SERS} is too elusive. Therefore we evaluated AEF to know the proportional enhancement. The AEF is evaluated in terms of ratio of integrated intensity (I_{SERS}/I_{NR}) called here as enhancement value (EV) under identical condition of measurement. The normal Raman bands at 1409 cm^{-1} and its corresponding SERS band at 1412 cm^{-1} are taken as reference bands to estimate the EF for calculating the EV. The calculated EV is 7.47 for PZCDT and 1.36 for PZbCDT. The concentration of solution is taken as 1M for normal Raman and 10^{-6} M for the SERS measurement in triple distilled water. Thus AEF for the SERS band is calculated to be of order of 10^6 .

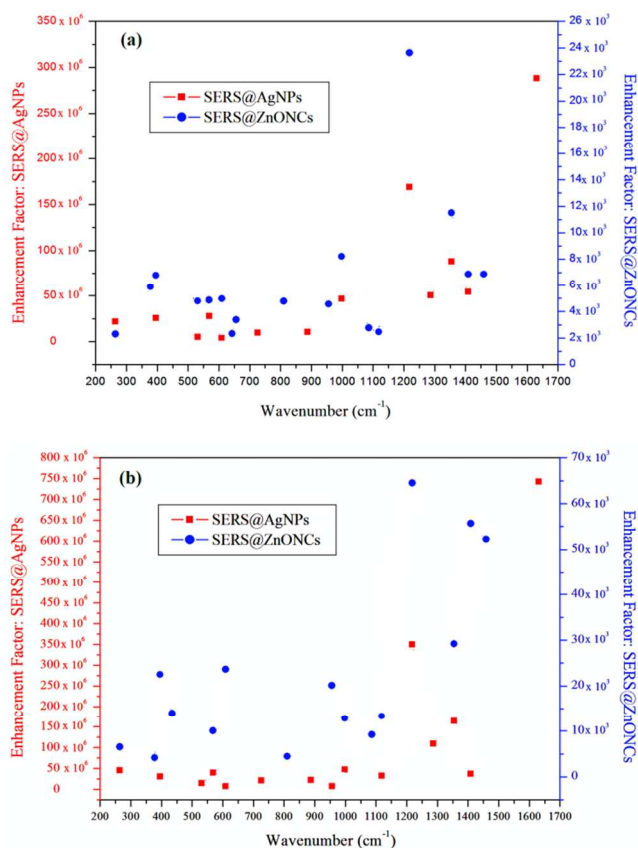


Fig. [7]: Comparative illustration (shown by points) of analytical enhancement factor between SERS@AgNPs and SERS@ZnONPs of vibrational modes of (a) PZCDT and (b) PZbCDT.

Similar method is followed to estimate AEF for SERS@ZnONPs as for SERS@AgNPs. The normal Raman bands at 264 cm^{-1} and its corresponding SERS band at 262 cm^{-1} are taken as reference bands. The calculated EV is 2.15 for PZCDT and 1.10 for PZbCDT. The AEF for the SERS band is calculated to be of the order of 10^3 . To compare the degree of enhancement from two substrates, we plotted the curves for SERS@AgNPs and SERS@ZnONPs observed in PZCDT and PZbCDT as shown in Fig. 7(a) and (b) respectively.

Conclusions:

In present work, we first of all investigated the adsorption geometry of analytes PZCDT/ PZbCDT on the two substrates AgNPs and ZnONPs from the intensity enhancement of SERS bands. In SERS@AgNPs, we perceived the growth of few new bands mainly at $1630, 1286, 888$ and 727 cm^{-1} . Two normal Raman bands at 380 and 401 cm^{-1} merged to 393 cm^{-1} in SERS spectra corresponding to $\delta_{ASYM}(\text{Ring})+\text{LIN}(\text{NCS})+\nu(\text{Ag-S})+\beta(\text{C-S-Ag})$, which confirms the formation of chemical bond (Ag-S). The absolutely different spectral features of SERS@ZnONPs and SERS@AgNPs characterized the unique signatures of two substrates; AgNPs and ZnONPs. The enhancement factor is found to be of order of 10^6 in SERS@AgNPs and 10^3 in SERS@ZnONPs. In SERS@ZnONPs, the bands at $436, 308, 241\text{ cm}^{-1}$ in PZbCDT and $307, 262\text{ cm}^{-1}$ in PZCDT give the clear evidence of chemical bond (Zn-S) formation. The adsorption of PZCDT and PZbCDT on AgNPs & ZnONPs via dithiocarbamate moiety as has shown the dithiocarbamate moiety as a competent functional group not only for AgNPs but also for ZnONPs.

Acknowledgement:

Om Prakash and PG (Senior Research Fellow) are grateful to the UGC, India for providing research fellowship. RKS is grateful to DFG & AvH Foundation, Germany, and DST and CSIR, New Delhi for financial support. Authors are also grateful to biophysics lab; Department of Physics and Department of Chemistry, BHU, Varanasi-221005, for providing lab facilities.

Experimental and Computational details:

Synthesis and characterization:

Piperazine and carbon disulfide were purchased from Sigma-Aldrich and used without further purification. All solvents purchased from Merck Chemicals, India were dried and distilled according to standard procedure.

PZCDT and PZbCDT were prepared according to literature methods.³⁹⁻⁴¹ For PZCDT, a mixture of PZ, KOH and CS_2 in ratio (1:1:1) was stirred for 4 hrs whereas for PZbCDT, a mixture of PZ, KOH and CS_2 in ratio (1:2:2) was stirred for 3 hrs & the resulting precipitates were filtered off & washed with diethylether, thereafter the resulting compounds were treated with dilute HCl in order to convert them into corresponding dithioic acids (PZCDT and PZbCDT). The silver island films were synthesized according to the procedure described in the literature.^{22, 42} The UV-Visible spectra and atomic force microscopy (AFM) image of silver island film as shown in Fig 8. The absorption band of silver island film is observed at $\sim 456\text{ nm}$

and film thickness is monitored ~ 6 nm as shown in Fig. 8. The surface topography of the prepared silver island film has been studied using AFM in the tapping mode. AFM data analysis gives the quantitative information about the surface morphology. The 2-dimensions (2D) AFM topography of silver island film (Fig. 8) clearly show that isolated silver particles are uniformly distributed over the glass substrate in nano-grained size with almost spherical shape.

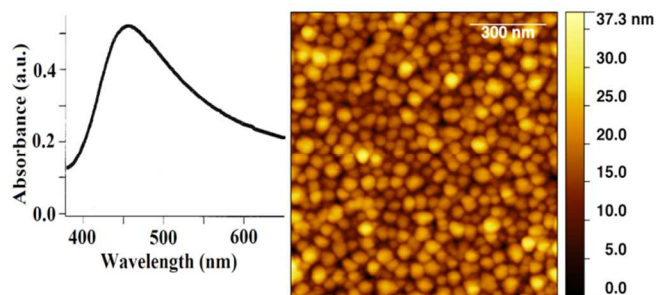


Fig 8: UV-Visible spectra and AFM image of as synthesized Ag island film.

The surface modification of AgNPs was done by the adsorption of analytes, PZCDT and PZbCDT. The solutions of PZDTC/PZbDTC (1.0×10^{-6} M conc.) were prepared in triple distilled water. 3 μ L of each solution (PZDTC/PZbDTC) is poured onto silver island film (AgNPs) and dried carefully. The Raman measurement was performed by focusing the laser spot on modified area. The ZnO nanoparticles (ZnONPs) were synthesized according to procedure given by S. Kumar et.al.⁴³ The synthesized ZnO nanoparticles were characterized by UV-Visible, XRD and Transmission electron microscope. The size of ZnO particles was estimated as 30 nm by XRD [ES1] and TEM analysis [ES2]. For the surface modification of ZnONPs, 8.1 mg of ZnONPs was dissolved in 10 ml of 1×10^{-3} M of PZDTC/PZbDTC and resulting mixture was stirred for 1 hour. Thereby obtained precipitate was rinsed with triple distilled water and thus obtained product was surface modified ZnONPs. The final product [ZnONPs + PZCDT/ PZbCDT] was characterized by UV-Visible, TEM and Raman measurements.

The laser Raman spectra were recorded on a Raman spectrometer from Renishaw Model: RM 1000 having grating of 2400 grooves/mm giving spectral resolution of 1 cm^{-1} and 514.5 nm Ar^+ as an excitation source. The absorption spectra were measured in the range of 300- 800 nm using UV-Visible spectrometer. TEM measurements were performed with JEOL-2010 (Japan). XRD analysis of ZnO nanoparticles was done by X-ray diffractometer (Model: Mini fl ex-II, Rigaku, Japan) with Cu $K\alpha$ radiation ($\lambda = 1.5406 \text{ \AA}$). The AFM measurement was performed with Nano Wizard atomic force microscope (resolution 10–20 μm), JPK Instrument AG, Germany.

DFT analysis:

According to the coordination chemistry, the most probable binding of PZCDT/ PZbCDT with the AgNPs surface takes place through the dithiocarbamate group showing either bidentate interaction or monodentate interaction as illustrated in Fig. 9.

To investigate the coordination properties of adsorbates

towards substrates (AgNPs/ZnONPs), the quantum chemical calculation has been employed with Gaussian 03 and GaussView 4.1 program packages. We have first investigated the possibility of bidentate and monodentate interaction exhibited between adsorbate and substrates. The geometry optimization of PZCDT/ PZbCDT with single Ag atom (deprotonated PZCDT/ PZbCDT + Ag_1) using DFT/ Lan12DZ method^{23-26, 44,45} suggested strongly for the possibility of bidentate interaction. Further we have performed the geometry optimizations of the complexes [PZCDT+ $\text{Ag}_{(n=2,3,4)}$] and [PZbCDT+ $\text{Ag}_{(n=2,3,4)}$] in bidentate form. The most possible optimized geometries of the PZCDT/ PZbCDT (also in deprotonated form) and its $\text{Ag}_{(n=1, 2, 3, 4)}$ complexes are as shown in Fig 2.

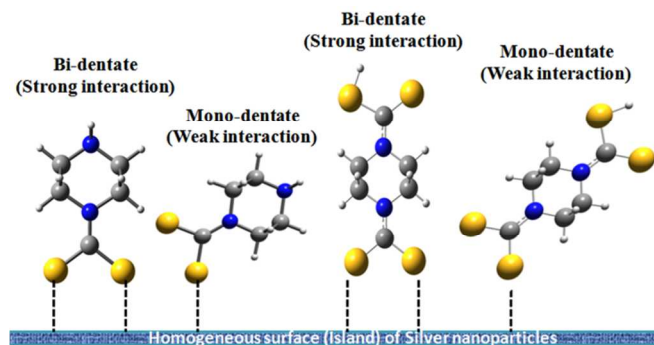


Fig. 9: Schematic demonstrations of possible interactions between adsorbates and silver islands (AgNPs).

To deduce the adsorption sites of PZCDT/PZbCDT on silver metal precisely, the molecular electrostatic potential surfaces (MEPS) have been also computed at the same level of DFT calculation as followed for the geometry optimization. MEPS are completely related to the electron density and a very useful descriptor for determining the sites for electrophilic attack and nucleophilic reaction as well as structure-reactivity relationship of the molecules.^{24, 46} The MEP surfaces of the optimized PZCDT/ PZbCDT ions and its $\text{Ag}_{(n=1, 2, 3, 4)}$ complexes are illustrated in Fig ES3. In Fig ES3, the electron density is localized mostly on both sulphur atoms of dithiocarbamate moiety, therefore electron deficient Ag atom interacts through the sulphur atoms of dithiocarbamate moiety. The DFT computation has been also performed to determine the adsorption sites of PZCDT/ PZbCDT on ZnONPs at the same level of calculation as followed for [PZCDT/ PZbCDT + AgNPs]. According to coordination chemistry of Zinc metal coordination of PZCDT and PZbCDT ions with the ZnONPs take place through the dithiocarbamate moiety showing bidentate interaction and construct a four membered chelate ring (Zn-S-C-S).^{47, 48} The most possible optimized structures and MEP surfaces of the [PZCDT + ZnONPs] and [PZbCDT + ZnONPs] are shown in Fig ES4.

Notes:

^a Department of Physics, Banaras Hindu University, Varanasi- 221105, India. Fax: +91 542 2368174; Tel: +91 542 6701569; E-mail: ranjankingsh65@rediffmail.com

^b Department of Chemistry, Banaras Hindu University, Varanasi- 221105, India.

^c Leibniz Institute of Photonic Technology, Albert-Einstein-Straße 9, 07745 Jena, Germany.

^d Institute of Physical Chemistry and Abbe Center of Photonics, Friedrich-Schiller University, Helmholtzweg 4, 07743 Jena, Germany

† Electronic Supplementary Information (ESI) available:

ES1- X-ray Diffraction analysis of synthesized ZnO:

Fig. (ES1) shows the Rietveld refinement of the X-ray diffraction (XRD) pattern for ZnO nanoparticles (NPs) synthesized by sol-gel method.

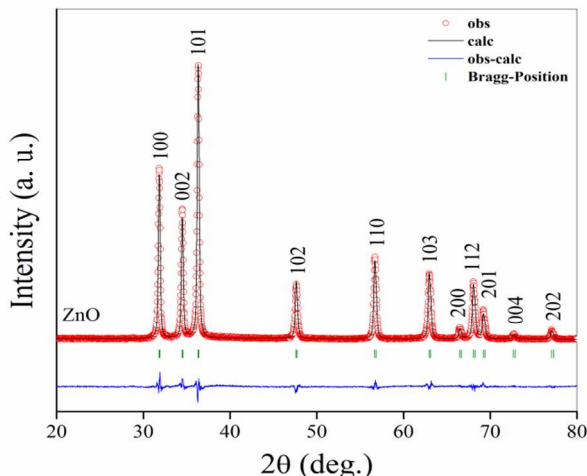


Fig ES1: XRD pattern of synthesized ZnO nanoparticles.

The well resolved peaks observed in the X-ray diffraction pattern indicate that ZnO NPs possess single phase. The red circles represent the observed data while solid line through red circles is the calculated profile. All peak positions of prepared ZnO NPs corresponding to the standard Bragg positions of hexagonal wurtzite ZnO (space group P63mc) have been shown by the vertical bars and the residue by the line respectively at the bottom of the XRD patterns and no trace of other impurities is found. The XRD pattern shows that the prepared ZnO has hexagonal wurtzite structure (with $a = b = 3.25 \text{ \AA}$, $c = 5.20 \text{ \AA}$) belonging to the C46v space group (P63mc) and indexed using the standard JCPDS file for ZnO (JCPDS 36-1451). The average grain size, D , of the ZnO NPs is estimated using the Debye-Scherrer's equation

$$\frac{0.9\lambda}{\beta \cos\theta}$$

where, D is the particle size, λ the wavelength of radiation used ($\lambda = 1.5406 \text{ \AA}$), θ the Bragg angle and β is the full width at half maxima (FWHM). The average crystallite size calculated by using the Debye-Scherrer's equation is 30 nm.

ES2: TEM and SEAD images of pure ZnONPs and [PZCDT/PZbCDT+ZnONPs]:

A typical TEM and SEAD (selected area electron diffraction) images of pure ZnONPs, complexes [PZCDT+ZnO] and [PZbCDT+ZnO] are presented in Fig. ES2. The ZnONPs are nearly spherical in shape with size between 20 and 30 nm. The average particle size obtained from TEM measurement matches well with size estimated from the XRD study. The selected area electron diffraction (SAED) pattern (Fig. ES2 (b)) shows the crystalline nature and the hexagonal-like shape of ZnONPs. Fig. ES2 (c), (d) and ES2 (e), (f) represents TEM and SAED image of complexes [PZCDT+ZnO] and [PZbCDT+ZnO] respectively. In

Fig. ES2(c) and ES2(e), we observed changes in TEM images of pure ZnONPs on adsorption of PZCDT and PZbCDT. Fig. ES2 (d) and ES2(f) show SAED images of complexes [PZCDT+ZnO] and [PZbCDT+ZnO] respectively.

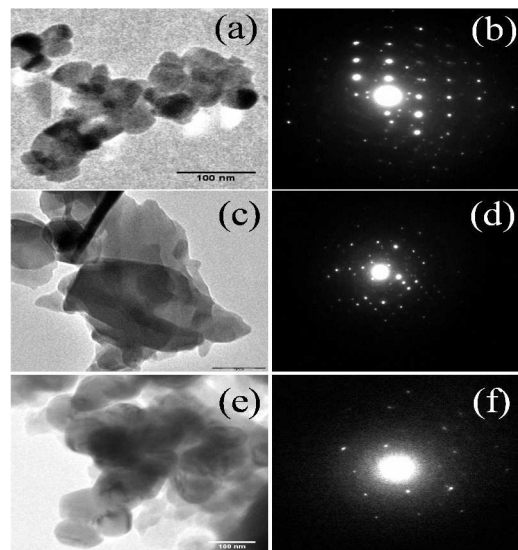


Fig.[ES2]: TEM images of (a) ZnONPs, (c) [PZCDT+ZnO], (e) [PZbCDT+ZnO], and SEAD images of (b) ZnONPs (d) [PZCDT+ZnO], (f) [PZbCDT+ZnO]

ES3: DFT calculated MEPS of PZCDT/ PZbCDT+Ag_{n=0, 1, 2, 3, 4}

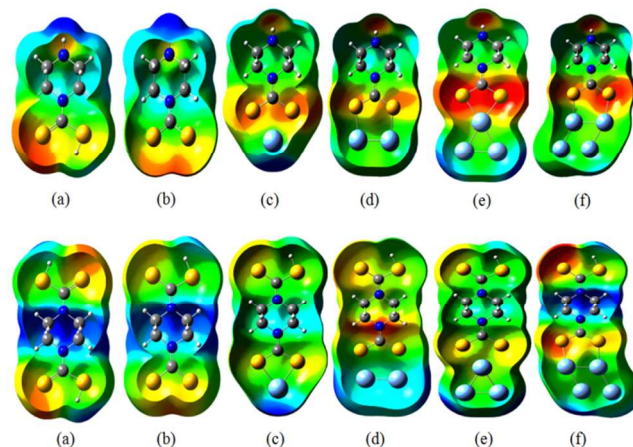


Fig ES3: Molecular electrostatic potential surfaces of optimized geometry of (a) PZCDT/PCbCDT, (b) deprotonated PZCDT/PCbCDT, (c) PZCDT/PCbCDT + Ag₁, (d) PZCDT/PCbCDT + Ag₂, (e) PZCDT/PCbCDT + Ag₃, (f) PZCDT/PCbCDT + Ag₄

ES4: DFT calculated MEPS of PZCDT/ PZbCDT+ZnO:

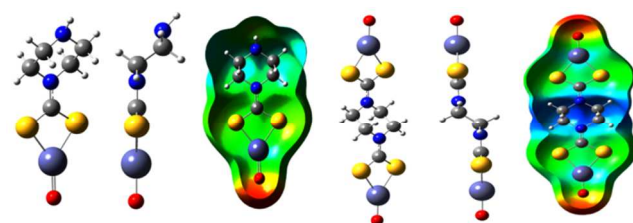


Fig ES4: Optimized structures of PZCDT +ZnO (a) front view, (b) side view, (c) MEPS of PZCDT +ZnO, and 4(ii) Optimized structures of PZbCDT +ZnO (a) front view, (b) side view, (c) MEPS of PZbCDT +ZnO.

5 See DOI: 10.1039/b000000x/

‡ Footnotes should appear here. These might include comments relevant to but not central to the matter under discussion, limited experimental and spectral data, and crystallographic data.

References:

- 10 (1) S. Nie and S. R. Emory, *Science*, 1997, 275, 1102-1106.
- (2) K. Kneipp, Y. Wang, H. Kneipp, L. T. Perelman, I. Itzkan, R. R. Dasari and M. S. Feld, *Physical Review Letters*, 1997, 78, 1667-1670.
- (3) K. Kneipp, Y. Wang, R. R. Dasari and M. S. Feld, *Appl. Spectrosc.*, 1995, 49, 780-784.
- 15 (4) K. Kneipp, H. Kneipp, R. Manoharan, I. Itzkan, R. R. Dasari and M. S. Feld, *Bioimaging*, 1998, 6, 104-110.
- (5) T. A. Alexander, *Analytical Chemistry*, 2008, 80, 2817-2825.
- (6) P. K. Jain, X. Huang, I. H. El-Sayed and M. A. El-Sayed, *Accounts of Chemical Research*, 2008, 41, 1578-1586.
- 20 (7) A. G. Brolo, D. E. Irish and B. D. Smith, *Journal of Molecular Structure*, 1997, 405, 29-44.
- (8) M. Moskovits, *Reviews of Modern Physics*, 1985, 57, 783-826.
- (9) H. Xu, E. J. Bjerneld, M. Käll and L. Börjesson, *Physical Review Letters*, 1999, 83, 4357-4360.
- 25 (10) A. Otto, I. Mrozek, H. Grabhorn and W. Akemann, *Journal of Physics: Condensed Matter*, 1992, 4, 1143.
- (11) D.-Y. Wu, J.-F. Li, B. Ren and Z.-Q. Tian, *Chemical Society Reviews*, 2008, 37, 1025-1041.
- (12) K. Saha, S. S. Agasti, C. Kim, X. Li and V. M. Rotello, *Chemical Reviews*, 2012, 112, 2739-2779.
- 30 (13) L. Chen, N. Qi, X. Wang, L. Chen, H. You and J. Li, *RSC Advances*, 2014, 4, 15055-15060.
- (14) J. R. Lombardi and R. L. Birke, *The Journal of Physical Chemistry C*, 2008, 112, 5605-5617.
- 35 (15) J. R. Lombardi, R. L. Birke, T. Lu and J. Xu, *The Journal of Chemical Physics*, 1986, 84, 4174-4180.
- (16) Zhao, L. Jensen and G. C. Schatz, *Journal of the American Chemical Society*, 2006, 128, 2911-2919.
- (17) M. Moskovits and J. S. Suh, *The Journal of Physical Chemistry*, 1984, 88, 5526-5530.
- 40 (18) M. Moskovits, D. P. DiLella and K. J. Maynard, *Langmuir*, 1988, 4, 67-76.
- (19) X. Gao, J. P. Davies and M. J. Weaver, *The Journal of Physical Chemistry*, 1990, 94, 6858-6864.
- 45 (20) M. Baia, L. Baia, W. Kiefer and J. Popp, *The Journal of Physical Chemistry B*, 2004, 108, 17491-17496.
- (21) M. Moskovits and D. H. Jeong, *Chemical Physics Letters*, 2004, 397, 91-95.
- (22) A. Rasmussen and V. Deckert, *Journal of Raman Spectroscopy*, 2006, 37, 311-317.
- 50 (23) T. d. F. Paulo, R. A. Ando, I. C. N. Diógenes and M. L. A. Temperini, *The Journal of Physical Chemistry C*, 2013, 117, 6275-6283.
- (24) D. Yang, N. E. Mircescu, H. Zhou, N. Leopold, V. Chiş, M. Oltean, Y. Ying and C. Haisch, *Journal of Raman Spectroscopy*, 2013, 44, 1491-1496.
- 55 (25) M.J. Frisch and J.A. Pople, Gaussian 03, Revision A.1, Gaussian Inc, Pittsburgh, 2003.
- (26) J.M.L. Martin and C. V. Alsenoy, GAR2PED, University of Antwerp, 1995.
- 60 (27) S. SenGupta, N. Maiti, R. Chadha and S. Kapoor, *Chemical Physics*, 2014, 436-437, 55-62.
- (28) D. C. N. B. F. W. G. G. J. G. Lin-Vien, The Handbook of infrared and raman characteristic frequencies of organic molecules, <http://site.ebrary.com/id/10699554>.
- 65 (29) V. Sathyanarayananmoorthi, R. Karunathan and V. Kannappan, *Journal of Chemistry*, 2013, 2013, 14.
- (30) C.-C. Li, S.-J. Chang, F.-J. Su, S.-W. Lin and Y.-C. Chou, *Colloids and Surfaces A: Physicochemical and Engineering Aspects*, 2013, 419, 209-215.
- 70 (31) A. Rahdar, *Journal of Nanostructure in Chemistry*, 2013, 3, 10.
- (32) M. Chen, Y.-G. Feng, X. Wang, T.-C. Li, J.-Y. Zhang and D.-J. Qian, *Langmuir*, 2007, 23, 5296-5304.
- (33) M. Cao, L. Zhou, X. Xu, S. Cheng, J.-L. Yao and L.-J. Fan, *Journal of Materials Chemistry A*, 2013, 1, 8942-8949.
- 75 (34) Persson, B. N. J. *Chem. Phys. Lett.* 1981, 82, 561.
- (35) A. Otto, "Surface-Enhanced Raman Scattering: 'Classical' and 'Chemical' Origins", in *Light Scattering in Solids IV*, M. Cardona and G. Guntherodt, Eds. (Springer-Verlag, Berlin, Germany, 1984), vol. 1984, p. 289.
- 80 (36) Z.-Q. Tian, B. Ren and D.-Y. Wu, *The Journal of Physical Chemistry B*, 2002, 106, 9463-9483.
- (37) J. Sarkar, J. Chowdhury and G. B. Talapatra, *The Journal of Physical Chemistry C*, 2007, 111, 10049-10061.
- 85 (38) W. Hossain, M. Ghosh, C. Sinha, D. K. Debnath and U. K. Sarkar, *Chemical Physics Letters*, 2013, 586, 132-137.
- (39) G. Rajput, V. Singh, A. N. Gupta, M. K. Yadav, V. Kumar, S. K. Singh, A. Prasad, M. G. B. Drew and N. Singh, *CrystEngComm*, 2013, 15, 4676-4683.
- 90 (40) A. N. Gupta, V. Singh, V. Kumar, A. Rajput, L. Singh, M. G. B. Drew and N. Singh, *Inorganica Chimica Acta*, 2013, 408, 145-151.
- (41) S. K. Singh, M. G. B. Drew and N. Singh, *CrystEngComm*, 2013, 15, 10255-10265.
- (42) R. M. Stöckle, V. Deckert, C. Fokas and R. Zenobi, *Appl. Spectrosc.*, 2000, 54, 1577-1583.
- 95 (43) S. Kumar, S. Chatterjee, K. K. Chattopadhyay and A. K. Ghosh, *The Journal of Physical Chemistry C*, 2012, 116, 16700-16708.
- (44) Y. Yang, M. N. Weaver and K. M. Merz, *The Journal of Physical Chemistry A*, 2009, 113, 9843-9851.
- 100 (45) N. Maiti, S. Thomas, J. A. Jacob, R. Chadha, T. Mukherjee and S. Kapoor, *Journal of Colloid and Interface Science*, 2012, 380, 141-149.
- (46) B. Galabov, S. Ilieva, G. Koleva, W. D. Allen, H. F. Schaefer Iii and P. von R. Schleyer, *Wiley Interdisciplinary Reviews: Computational Molecular Science*, 2013, 3, 37-55.
- 105 (47) M. S. Thomas, D. C. Liles, M. Landman, E. M. van der Merwe and S. Lotz, *Polyhedron*, 2006, 25, 3562-3568.
- (48) V. Milacic, D. Chen, L. Giovagnini, A. Diez, D. Fregona and Q. P. Dou, *Toxicology and Applied Pharmacology*, 2008, 231, 24-33.